 CMES, vol.86, no.6, pp.505-531, 2012

Analysis for Shakedown of Functionally Graded Plate Subjected to Thermal-Mechanical Loading with Piecewise-Exponential Distribution of Material Properties

H. Zheng[1], X. Peng[1,2,3] and N. Hu[1,4]

Abstract: The static and kinematic shakedown of a functionally graded plate (FGP) is analyzed. The FGP is subjected coupled constant mechanical load and cyclically varying temperature. The FGP is composed of elastoplastic matrix and elastic particles, with the particle volume fraction varying along its thickness. The thermal and mechanical properties and their distributions are evaluated with a mean filed approach, which is based on the Eshelby's inclusion theory and takes into account directly the interaction between particles. The FGP is assumed to be separated into a number of thin layers, the thermal and mechanical properties in the thickness direction of each layer are assumed to vary exponentially over the layer thickness and continuum between neighboring layers. The above piecewise exponential modeling can replicate the actual distribution of the material properties of the FGP with sufficient accuracy. The boundaries between the shakedown area and the areas of elasticity, incremental collapse and reversed plasticity are determined. The shakedown of its homogeneous counterpart with averaging material properties is also analyzed. The comparison between the results obtained in the two cases exhibits distinctly qualitative and quantitative difference, indicating the importance of a proper shakedown analysis for the FG plate. The approach developed in this article can be used not only for the analysis of the shakedown of FGPs with high accuracy, but also for the optimum design of the FGPs, e.g., the optimization of the distribution of the material properties.

[1] Department of Engineering Mechanics, Chongqing University, Chongqing, China

[2] State Key Laboratory of Coal Mine Disaster Dynamics and Control, Chongqing University, Chongqing, China

[3] Corresponding author: X. Peng, Address: Department of Engineering Mechanics, Chongqing University, Chongqing, 400044, China. Tel.: +86 23 6510 2421; fax: +86 23 6510 2421. *E-mail address*: xhpeng@cqu.edu.cn.

[4] Corresponding author: N. Hu, Address: Department of Mechanical Engineering, Chiba University, Chiba, 263-8522 Japan. Tel. and Fax: +81 43 290 3204. *E-mail address*: huning@faculty.chiba-u.jp.

Keywords: functionally graded plate, coupled thermal-mechanical loading, piecewise exponential distribution of material properties, mean-field approach, shakedown

1 Introduction

Functionally graded materials (FGMs) are a class of advanced composites characterized by the gradual variation in composition, microstructure and material properties [Reddy (2004); Hasselman et al. (1978); Yamanouchi et al. (1990); Koizumi (1993)]. FGMs were proposed initially as thermal barrier materials for applications in space planes, space structures, nuclear reactors, turbine rotors, flywheels, gears, etc.

The development achieved in recent years implies the great potential of FGMs in a wide range of thermal, biomedical and structural applications [Suresh et al. (1998); Watari et al. (2004); Reddy (2011)], and plate structures made of FGMs have also been widely used in practical engineering. Great progress has been made in the research in the mechanical properties of functionally graded plates (FGPs), such as buckling, bending and vibration [Feldoman et al. (1997); Na and Kim (2006); Aghabaei and Reddy (2009); Altenbach and Eremeyev (2009); Wu and Huang (2009); Hosseini et al. (2011)], cracking and thermal fracture [Wang et al (2000); Guo et al. (2005)], transient thermal stress [Cheng and Batra (2000); Vel and Batra (2002, 2003); Andrew and Senthil (2010)], static and dynamic responses [Zhong and Shang (2003); Elishakoff and Gentilini (2005); Gilhooley et al. (2007)], shakedown [Peng et al. (2009a, 2009b)], etc.

The shakedown of functionally graded (FG) structures is an essential problem for the structures subjected to coupled varying thermal and mechanical loadings. In the initial work [Peng et al. (2009b)], the shakedown of the FG Bree plates was investigated, where the thermal-mechanical properties of the material was assumed to distribute exponentially over the thickness of the plate, which may result in marked error if the distribution of the actual material properties is markedly different from this assumption.

The description of the distributions of material properties is significantly important in the analysis of the mechanical behavior of FGM structures. It was pointed out [Zuiker (1995)] that the assumed property distributions must be used with care, because they may not be physically reliable for certain material-combination. In most of the articles mentioned above, the material properties distributions of FGMs were usually described with a single function in plate thickness, such as the linear function, the power-law function, or the exponential function, etc. However, in most cases, the actual properties of practical FGMs can hardly be replicated with

these predefined single distributions. Therefore, it is necessary to develop some approaches which can describe realistically the properties of FGMs with arbitrary distribution. The piecewise-exponential distribution model [Guo and Noda (2007, 2008a); Guo et al. (2008b)] can provide a satisfactory solution, for it can approach arbitrary distributions of different properties of FGPs with sufficient accuracy. On the other hand, the concept of the piecewise-distribution model also coincides with the adopted discrete numerical approach. Therefore, there should be no additional difficulties for such kind of distributions to be applied in analysis.

In order to make the shakedown analysis more physically reliable, in this article, the thermal-mechanical properties in an FG plate is evaluated with a mean filed approach that is based on the Eshelby's inclusion theory by taking into account directly the interaction between particles. The distribution of the material properties is assumed piecewise exponential over the thickness of the plate, which can replicate the actual distribution of the material properties with sufficient accuracy. The shakedown boundaries related to incremental collapse and reversed plasticity are analyzed with the static and kinematic shakedown theorems.

2 Brief introduction to constitutive model and static and kinematic shakedown theorems

Assuming small deformation, for initially isotropic and plastically incompressible materials, the constitutive model adopted can be expressed as

$$\varepsilon_{ij} = \varepsilon_{ij}^{e} + e_{ij}^{p} + \varepsilon_{ij}^{\theta}, \tag{1}$$

where ε_{ij} is strain and $\varepsilon_{ij}^{e}, e_{ij}^{p}$ and $\varepsilon_{ij}^{\theta}$ are its elastic, plastic and thermal components, respectively, which are determined with

$$\varepsilon_{ij}^{e} = \frac{1}{E}\left[(1+\nu)\sigma_{ij} - \nu\sigma_{kk}\delta_{ij}\right], \quad \varepsilon_{ij}^{\theta} = \alpha(\theta-\theta_0)\delta_{ij}, \quad de_{ij}^{p} = d\lambda s_{ij}, \tag{2}$$

where E, ν and α are the Young's modulus, the Poisson's ratio and the coefficient of linear expansion, respectively, σ_{ij} and s_{ij} are stress and its deviatoric component, θ and θ_0 are temperature and reference temperature, respectively, δ_{ij} is the Kronecker delta, and

$$d\lambda = \frac{d\zeta}{f(\lambda)s_y^0}, \tag{3}$$

with $d\zeta = \sqrt{de_{ij}^{p} de_{ij}^{p}}$.

s_y^0 is a material constant related to initial yield and $f(\lambda) > 0$ is a function describing the isotropic hardening [Peng et al. (1996)]. It can be seen that $d\lambda$ is non-negative in any plastic deformation process. The following hardening function will be adopted in the following analysis,

$$f(\lambda) = d - (d-1)e^{-\beta\lambda} \tag{4}$$

with $f(0) = 1$ and $d \geq 1$.

It can be seen in Eqs. (3) and (4) that $f(\lambda)$ increases with the development of plastic deformation and tends to its asymptotic value d corresponding to the ultimate strength $\sigma_y = d \cdot \sigma_y^0$ as plastic deformation fully develops when $\lambda \to \infty$, indicating a saturated state of isotropic hardening. Substituting Eq. (3) into Eq. $(2)_3$ yields the following Mises-type yield condition

$$s_{ij}s_{ij} = \left[f(\lambda)s_y^0\right]^2. \tag{5}$$

Introducing the following loading function

$$F(s_{ij},k) = \sqrt{s_{ij}s_{ij}} - ks_y^0, \tag{6}$$

with $1 \leq k \leq d$.

It can be seen that any state of stress should satisfy $F(s_{ij},k) \leq 0$, and $F(s_{ij},k) = 0$ defines a loading surface.

Given a set of actual stress and hardening states, s_{ij} and k, and a set of allowable stress and hardening states, s_{ij}^*, k^*, which satisfy

$$\begin{aligned} &F(s_{ij},k) = 0, \quad 1 \leq k \leq d, \\ &F\left(s_{ij}^*,k^*\right) \leq 0, \quad 1 \leq k^* \leq d, \end{aligned} \tag{7}$$

and making use of the following inequality

$$(s_{ij} - s_{ij}^*)de_{ij}^p \geq 0, \tag{8}$$

one can prove that [Peng and Ponter (1993)]

$$(s_{ij}^* - s_{ij})de_{ij}^p \leq s_y^0(k^* - k)d\zeta. \tag{9}$$

2.1 Static Shakedown Theorem [Peng et al (2009a, 2009b)]

If there exist a time-independent residual stress field $\bar{\rho}_{ij}$ and a time-independent field k^* such that for all the load variations within a given load domain Ω, the following condition holds

$$F\left(s_{ij}^E + \bar{\rho}_{ij}, k^*\right) \leq 0 \tag{10}$$

then the total energy dissipated in any allowable load path is bounded.

In Eq. (10) s_{ij}^E is the purely elastic solution of the deviatoric stress determined by external loads and $1 \leq k^* \leq d$.

2.2 Kinematic Shakedown Theorem [Peng et al (2009a, 2009b)]

If there exist, over a certain time interval (t_1,t_2), a history of load resulting in a history of purely elastic stress $s_{ij}^E(\mathbf{x},t)$, and a history of plastic strain $\bar{e}_{ij}(\mathbf{x},t)$ resulting in a kinematically admissible increment such that

$$\Delta\bar{e}_{ij}(\mathbf{x}) = \bar{e}_{ij}(\mathbf{x},t_2) - \bar{e}_{ij}(\mathbf{x},t_1) = \frac{1}{2}(\Delta\bar{u}_{i,j} + \Delta\bar{u}_{j,i}), \tag{11}$$

with $\Delta\bar{u}_i = 0$ on S_u(the boundary where displacement is prescribed), and if shakedown occurs in the given structure, the condition

$$\int_{t_1}^{t_2}\int_V s_{ij}^E(\mathbf{x},t)\dot{\bar{e}}_{ij}(\mathbf{x},t)dVdt \leq \int_{t_1}^{t_2}\int_V D(\dot{\bar{e}}_{ij}(\mathbf{x},t))\,dVdt \tag{12}$$

should be satisfied for all kinematically admissible plastic strain cycles.

In Ineq. (12),

$$D(\dot{\bar{e}}_{ij}(\mathbf{x},t)) = \bar{s}_{ij}(\mathbf{x},t)\dot{\bar{e}}_{ij}(\mathbf{x},t) \tag{13}$$

is a dissipation function.

The following relationship can be obtained for practical application by substituting Eqs. $(2)_3$and (3) into Ineq. (12) by following the definition by König [(1987)],

$$\int_V d\cdot s_y^0\Delta\bar{\xi}dV - \sum_{k=1}^{m}\int_V \alpha_k(\mathbf{x})J_k(\mathbf{x})dV \geq 0 \tag{14}$$

where

$$\Delta\bar{\xi} = \left\|\Delta\bar{e}_{ij}\right\|, \quad J_k(\mathbf{x}) = s_{ij}^E(\mathbf{x})\Delta\bar{e}_{ij}(\mathbf{x}), \quad \alpha_k = \begin{cases}\beta_k^+ & \text{if } J_k(\mathbf{x}) > 0\\ \beta_k^- & \text{if } J_k(\mathbf{x}) < 0\end{cases} \tag{15}$$

and a set of inequalities $\beta_k^- \leq \beta_k \leq \beta_k^+$($k$=1,2,...,$m$) defines the domain Ω of loads.

3 Shakedown of an FG plate

3.1 The Bree plate

A plate (Fig. 1) of thickness h is subjected to loads (P_x, P_y) per unit length in two mutually orthogonal directions. The surfaces of the plate are subjected to temperatures θ_2 and θ_1 which vary cyclically as shown in Fig. 1. The cycle time Δt is

assumed large compared with characteristic heat conduction time, and the change, between θ_0 (a reference temperature) and $\theta_0 + \Delta\bar{\theta}$, is assumed to take place sufficiently slowly for steady state conditions of prevail. The strain ε_x and ε_y are assumed to be uniform throughout the thickness of the plate. This problem is a simulation of the behavior of a thin walled tube, in the context of a nuclear fuel can design problem by Bree (1967) for homogeneous material and perfect plasticity.

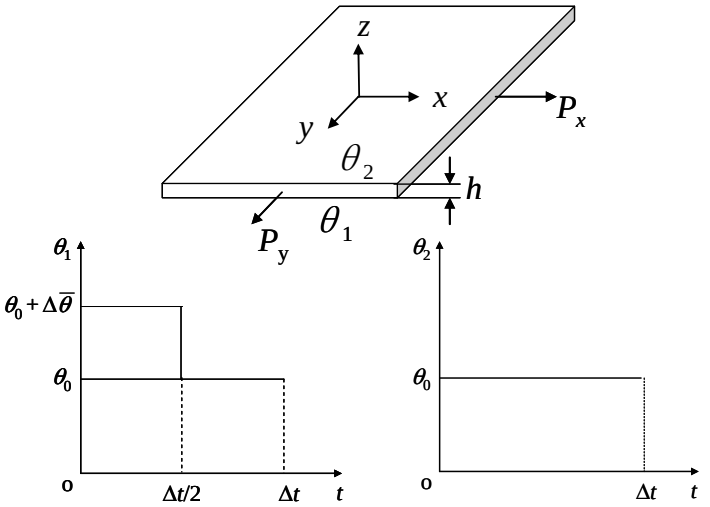

Figure 1: The Bree plate

3.2 PWED model and material properties

The piece-wise exponential distribution model (PWED model) [Guo et al. (2007)] is adopted for the distribution of the material properties in an FG plate, as shown in Fig. 2. The plate is assumed to be divided into L inhomogeneous layers in the direction of thickness, in each of which the thermal-mechanical properties vary exponentially. By this way, the actual thermal-material properties of the plate can be approximated with a set of exponential functions. At both surfaces of a layer the properties are identical with the actual properties of the material. Therefore, the properties of an FG plate can be approximated with sufficient accuracy if the thickness of each layer is sufficiently small.

The plate of thickness h is assumed to be divided into L layers, each of which is marked with a subscript $i(i = 1,2,\ldots, L)$, counting from the bottom surface of the

plate, the i-th layer is located between z=h_{i-1} and z=h_i, and at the bottom surface h_0=-h/2, while at the top surface h_L= h/2. Suppose $f_P(z)$ is the real distribution of a thermal/mechanical property in a layer, we can approximate $f_P(z)$ with $P(z)$, i.e.,

$$P(z) \approx f_P(z). \tag{16}$$

We further assume

$$P_i(z) = P_{i0} e^{\delta_i^P (z-h_{i-1})}, \quad i = 1,\ldots,L,\ h_{i-1} \le z \le h_i \tag{17a}$$

where

$$\begin{cases} P_i(h_{i-1}) = f_P(h_{i-1}), \\ P_i(h_i) = f_P(h_i). \end{cases} \quad i = 1,2,...,L. \tag{17b}$$

Given a set of actual values of a thermal/mechanical property, $f_P(h_i)$, i=0,1,…,L, for each segment P_{i0} and δ_i^P can be solved from Eqs. (17a) and (17b) as

$$P_{i0} = f_P(h_{i-1}) \text{ and } \delta_i^P = \frac{1}{h_i - h_{i-1}} \ln\left[\frac{f_P(h_i)}{f_P(h_{i-1})}\right]. \tag{18}$$

Substituting Eq.(18) into Eq.(17a) one obtains

$$P_i(z) = a_{Pi}(b_{Pi})^z, \quad i = 1,\ldots,L,\ h_{i-1} \le z \le h_i \tag{19a}$$

$$a_{Pi} = f_P(h_i)\left[f_P(h_i)/f_P(h_{i-1})\right]^{-\frac{h_i}{h_i - h_{i-1}}}, \quad b_{Pi} = \left[f_P(h_i)/f_P(h_{i-1})\right]^{\frac{1}{h_i - h_{i-1}}} \tag{19b}$$

where P can be replaced respectively with the Young's modulus E, the coefficient of thermal expansion α, thermal conductivity λ, yield stress σ_y^0, etc., i.e.,

$$E_i(z) = a_{Ei}(b_{Ei})^z \quad i = 1,\ldots,L,\ h_{i-1} \le z \le h_i \tag{20a}$$

$$a_{Ei} = f_E(h_i)\left[f_E(h_i)/f_E(h_{i-1})\right]^{-h_i/(h_i - h_{i-1})}, \quad b_{Ei} = \left[f_E(h_i)/f_E(h_{i-1})\right]^{1/(h_i - h_{i-1})} \tag{20b}$$

$$\sigma_{yi}^0(z) = a_{yi}(b_{yi})^z, \quad i = 1,\ldots,L,\ h_{i-1} \le z \le h_i \tag{21a}$$

$$a_{yi} = f_y(h_i)\left[f_y(h_i)/f_y(h_{i-1})\right]^{-h_i/(h_i - h_{i-1})}, \quad b_{yi} = \left[f_y(h_i)/f_y(h_{i-1})\right]^{1/(h_i - h_{i-1})} \tag{21b}$$

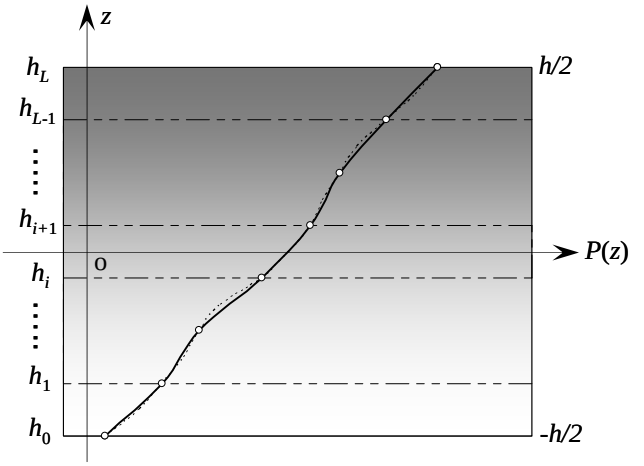

Figure 2: Piecewise-exponential distribution model for FG plate with arbitrarily distributed properties

$$\alpha_i(z) = a_{\alpha i}(b_{\alpha i})^z \quad i = 1,\ldots,L,\ h_{i-1} \le z \le h_i \tag{22a}$$

$$a_{\alpha i} = f_\alpha(h_i)\left[f_\alpha(h_i)/f_\alpha(h_{i-1})\right]^{-h_i/(h_i-h_{i-1})}, \quad b_{\alpha i} = \left[f_\alpha(h_i)/f_\alpha(h_{i-1})\right]^{1/(h_i-h_{i-1})} \tag{22b}$$

$$\lambda_i(z) = a_{\lambda i}(b_{\lambda i})^z \quad i = 1,\ldots,L,\ h_{i-1} \le z \le h_i \tag{23a}$$

$$a_{\lambda i} = f_\lambda(h_i)\left[f_\lambda(h_i)/f_\lambda(h_{i-1})\right]^{-h_i/(h_i-h_{i-1})}, \quad b_{\lambda i} = \left[f_\lambda(h_i)/f_\lambda(h_{i-1})\right]^{1/(h_i-h_{i-1})} \tag{23b}$$

Considering that the variation of the Poisson's ratio in each layer is insignificant and in order to simplify the analysis, we assume the Poisson's ratio in each layer is a constant taking the mean of the Poisson's ratio over the thickness, i.e.,

$$\nu = \frac{1}{L+1}(\bar{\nu}_0 + \bar{\nu}_1 + \ldots + \bar{\nu}_{i-1} + \ldots + \bar{\nu}_L), \quad i = 1,\ldots,L. \tag{24}$$

3.3 A mean-field approach for FGM considering particles interactions

An available mean-field approach may play a key role in evaluating realistically the effective properties of a composite. Conventional approaches such as the Mori-Tanaka method [Mori and Tanaka (1973)] and the self-consistent method [Hill

(1963); Budiansky (1965)] can directly be applied to estimate the effective elastic responses of FGMs [Suresh and Mortensen (1998); Miyamoto et al. (1999); Zuiker (1995); Gasik (1998); Vel and Batra (2003); Kim and Paulino (2003)]. It was noted [Yin et al. (2004, 2005)] that these approaches were originally developed for homogeneous mixtures with constant particle concentration, and no direct interactions between particles are taken into consideration [Zuiker and Dvorak (1994)]. Some researchers suggested higher-order theory in the modeling for FGMs [Aboudi et al. (1999); Reiter and Dvorak (1997, 1998)], but these methods are computationally intensive and inconvenient to be implemented in analysis [Yin et al. (2004, 2005)]. The mean-field approaches, which takes into account the pair-wise interaction between particles [Ju et al. (1994a, 1994b, 1994c); Yin et al (2004, 2005)], proved efficient and will be adopted in the evaluation of $f_E(z)$ and $f_y(z)$.

Suppose the particle volume fraction at z is $\xi(z)$, the effective properties can be determined with

$$\bar{K}(z) = K_m \left\{ 1 + \frac{30\xi(z)(1-\nu_m)(3\gamma_1+2\gamma_2)}{3\alpha'+2\beta-10\xi(z)(1+\nu_m)(3\gamma_1+2\gamma_2)} \right\} \tag{25}$$

$$\bar{\mu}(z) = \mu_m \left\{ 1 + \frac{30\xi(z)(1-\nu_m)\gamma_2}{\beta-4\xi(z)(5-5\nu_m)\gamma_2} \right\} \tag{26}$$

$$f_E(z) = \bar{E}(z) = \frac{9\bar{K}(z)\bar{\mu}(z)}{3\bar{K}(z)+\bar{\mu}(z)} \tag{27}$$

$$\bar{\nu}(z) = \frac{3\bar{K}(z)-2\bar{\mu}(z)}{6\bar{K}(z)+2\bar{\mu}(z)} \tag{28}$$

$$f_y(z) = \bar{\sigma}_y^0(z) = \sqrt{\frac{2}{3}} \frac{\sigma_{my}}{[1-\xi(z)]\sqrt{\bar{T}_1(z)+2\bar{T}_2(z)}}, \quad \bar{\sigma}_y(z) = k^* \bar{\sigma}_y^0(z) \tag{29}$$

where

$$\begin{aligned} \alpha' &= 2(5\nu_m-1)+10(1-\nu_m)\left(\tfrac{K_m}{K_c-K_m}-\tfrac{\mu_m}{\mu_c-\mu_m}\right), \\ \beta &= 2(4-5\nu_m)+15(1-\nu_m)\tfrac{\mu_m}{\mu_c-\mu_m}; \end{aligned} \tag{30}$$

$$\begin{aligned} \gamma_1(z) &= \tfrac{5\phi(z)}{4\beta^2}\left[-5\nu_m^2+2\nu_m-2-\tfrac{4\alpha'(1-2\nu_m)(1+\nu_M)}{3\alpha'+2\beta}\right], \\ \gamma_2(z) &= \tfrac{1}{2}+\tfrac{5\phi(z)}{8\beta^2}\left[5\nu_m^2-11\nu_m+11-\tfrac{3\alpha'(1-2\nu_m)(1+\nu_m)}{3\alpha'+2\beta}\right]; \end{aligned} \tag{31}$$

$$\begin{aligned} \bar{T}_1(z) &= \tfrac{3T_1(z)+2T_2(z)}{3[1+a(z)\xi(z)]^2}-\tfrac{2T_2(z)}{3[1+b(z)\xi(z)]^2}, \\ \bar{T}_2(z) &= \tfrac{T_2(z)}{[1+b(z)\xi(z)]^2}; \end{aligned} \tag{32}$$

$$\begin{aligned} &3T_1(z)+2T_2(z)=200\left(1-2\nu_m\right)^2\frac{\xi(z)}{(3\alpha'+2\beta)^2},\\ &T_2(z)=\tfrac{1}{2}+\left(23-50\nu_m+35\nu_m^2\right)\frac{\xi(z)}{\beta^2}; \end{aligned} \tag{33}$$

and

$$a(z)=20\left(1-2\nu_m\right)\frac{3\gamma_1(z)+2\gamma_2(z)}{3\alpha'+2\beta},\quad b(z)=\left(7-5\nu_m\right)\frac{2\gamma_2(z)}{\beta}, \tag{34}$$

where the subscript "m" and "c" denote matrix and inclusion, respectively, K_m, K_c and $\bar{K}$ are the bulk moduli of the matrix, the inclusion, and the composite, respectively, μ_m, μ_c and $\bar{\mu}$ are shear moduli of the matrix, the inclusion, and the composite, respectively.

There are some work related to the coefficient of thermal expansion and thermal conductivity of FGMs. Tian et al (2009, 2010) analyzed the heat conduction problem of FGMs using the hybrid numerical method. Yin et al. (2005, 2007) computed the coefficient of thermal expansion and thermal conductivity with a micromechanics method. Here, we determine the coefficient of thermal expansion α and the thermal conductivity λ at z using the method [Shen (1998)]

$$f_\alpha(z)=\bar{\alpha}(z)=\alpha_m+\frac{\left(1/\bar{K}(z)-1/K_m\right)\left(\alpha_c-\alpha_m\right)}{1/K_c-1/K_m}, \tag{35}$$

$$f_\lambda(z)=\bar{\lambda}(z)=\lambda_m\left[1+\frac{3\xi(z)\left(\lambda_c/\lambda_m-1\right)}{3-\left[1-\xi(z)\right]\left(\lambda_c/\lambda_m-1\right)}\right] \tag{36}$$

The corresponding properties at $z=h_i$ (i=0, 1, 2, …, L) can be obtained as

$$f_E(h_i)=\bar{E}(h_i),\quad f_{\sigma_y^0}(h_i)=\bar{\sigma}_y^0(h_i),\quad f_\alpha(h_i)=\bar{\alpha}(h_i),\quad f_\lambda(h_i)=\bar{\lambda}(h_i). \tag{37}$$

It should be noted that the thermal/mechanical properties of an FGP can also be obtained with the composite with the identical constituents (identical matrix, inclusion particles and volume fractions). With the obtained results, the distribution of the Young's modulus $E(z)$ in the FGM can be obtained by interpolation with Eqs. (20) and (27), the Poisson's ratio $\nu(z)$ by Eqs. (24) and (28), the yield strength $\sigma_y^0(z)$ by Eqs. (21) and (29), the coefficient of thermal expansion $\alpha(z)$ by Eqs.(22) and (35), and the thermal conductivity $\lambda(z)$ by Eqs.(23) and (36).

3.4 Temperature distribution

Assuming steady-state heat transfer, the distribution of the temperature in a structure can be described with the following heat conduction equation without considering source heat,

$$\nabla\cdot\{\lambda(\mathbf{x})\nabla\theta\}=0 \tag{38}$$

For uniaxial heat transfer, as shown in Fig. 3, Eq. (38) can be simplified as

$$\frac{d}{dz}\left\{\lambda(z)\frac{d\theta}{dz}\right\}=0 \tag{39}$$

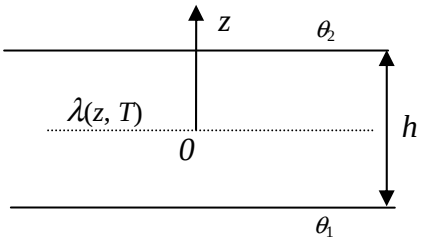

Figure 3: Heat transfer in Bree plate

Then we can obtain

$$\theta(z)=\theta_2+(\theta_1-\theta_2)\left[\int_z^{h/2}\frac{1}{\lambda(z)}dz\Big/\int_{-h/2}^{h/2}\frac{1}{\lambda(z)}dz\right]. \tag{40}$$

Letting $\Delta\tilde{\theta}=\theta_1-\theta_2$, $\Delta\theta(z)=\theta(z)-\theta_2$ can be obtained as

$$\Delta\theta(z)=\Delta\tilde{\theta}\left[1-\int_{-h/2}^{z}\frac{1}{\lambda(z)}dz\Big/\int_{-h/2}^{h/2}\frac{1}{\lambda(z)}dz\right] \tag{41a}$$

For the temperature distribution in the Bree plate (Fig.1), one can obtain

$$\Delta\tilde{\theta}=\begin{cases}\Delta\bar{\theta} & n\Delta t\le t\le(n+0.5)\Delta t\\ 0 & (n+0.5)\Delta t\le t\le(n+1)\Delta t\end{cases} \tag{41b}$$

Substituting Eq. (24a) into (42a), one has

$$\begin{aligned}\int_{-h/2}^{z}\frac{1}{\lambda(z)}dz&=\sum_{j=1}^{i-1}\int_{h_{j-1}}^{h_j}\frac{1}{\lambda_j(z)}dz+\int_{h_{i-1}}^{z}\frac{1}{\lambda_i(z)}dz\\&=\sum_{j=1}^{i-1}\frac{-\left(b_{\lambda j}^{-h_j}-b_{\lambda j}^{-h_{j-1}}\right)}{a_{\lambda j}Inb_{\lambda j}}+\frac{b_{\lambda i}^{-h_{i-1}}}{a_{\lambda i}Inb_{\lambda i}}-\frac{b_{\lambda i}^{-z}}{a_{\lambda i}Inb_{\lambda i}}\end{aligned}, \tag{42a}$$

i=1, …, L,

$$\int_{-h/2}^{h/2}\frac{1}{\lambda(z)}dz=\sum_{i=1}^{L}\int_{h_{i-1}}^{h_i}\frac{1}{\lambda_i(z)}dz=\sum_{i=1}^{L}\frac{-\left(b_{\lambda i}^{-h_i}-b_{\lambda i}^{-h_{i-1}}\right)}{a_{\lambda i}Inb_{\lambda i}}, \tag{42b}$$

i=1, ..., L, and $\Delta\theta_i(z)$ can be obtained as

$$\Delta\theta_i(z) = \Delta\tilde{\theta}\left(a_{\theta i} + b_{\theta i} b_{\lambda i}^{-z}\right), \tag{43a}$$

i=1, ..., L,

$$a_{\theta i} = 1 - \left(\sum_{j=1}^{i-1} \frac{-\left(b_{\lambda j}^{-h_j} - b_{\lambda j}^{-h_{j-1}}\right)}{a_{\lambda j} Inb_{\lambda j}} + \frac{b_{\lambda i}^{-h_{i-1}}}{a_{\lambda i} Inb_{\lambda i}} \right) \Big/ \left(\sum_{i=1}^{L} \frac{-\left(b_{\lambda i}^{-h_i} - b_{\lambda i}^{-h_{i-1}}\right)}{a_{\lambda i} Inb_{\lambda i}} \right) \tag{43b}$$

$$b_{\theta i} = \frac{1}{a_{\lambda i} Inb_{\lambda i} \left(\sum\limits_{i=1}^{L} \frac{-\left(b_{\lambda i}^{-h_i} - b_{\lambda i}^{-h_{i-1}}\right)}{a_{\lambda i} Inb_{\lambda i}} \right)}. \tag{43c}$$

3.5 Purely elastic solution

For the FG Bree plate, we will be concerned with the solution when the displacement in y-direction is fixed, i.e., ε_y=0, for simplicity. In this case, we need not be concerned with the yield condition in y-direction [Bree (1967]]. The components of the strain in the plate subjected to stress σ_x, σ_y can be expressed as

$$\varepsilon_x - \alpha(z)\Delta\theta(z) = \frac{1}{E(z)}(\sigma_x - \nu\sigma_y) \tag{44a}$$

$$\varepsilon_y - \alpha(z)\Delta\theta(z) = \frac{1}{E(z)}(\sigma_y - \nu\sigma_x) \tag{44b}$$

where $\Delta\theta(z)$ is the temperature change at z. Keeping in mind that ε_y=0, it can be solved from Eq. (44a) that

$$\sigma_x = \frac{E(z)}{1-\nu^2}\left[\varepsilon_x - \alpha(z)(1+\nu)\Delta\theta(z)\right]. \tag{45}$$

(1) Purely elastic solution of the stress distribution σ_P caused by P_x

When P_x is applied individually, i.e., $\Delta\theta(z)$=0, the equilibrium in x-direction gives

$$\int_{-h/2}^{h/2} \sigma_p dz = \int_{-h/2}^{h/2} \frac{E(z)}{1-\nu^2}\varepsilon_x dz = P_x. \tag{46}$$

Substitute Eq. (45) and $\Delta\theta(z)$=0 into Eq. (46), we obtain $\varepsilon_x = \varepsilon_0 = \frac{P_x}{\int_{-h/2}^{h/2} \frac{E(z)}{1-\nu^2} dz}$. Keeping in mind that ν can be treated as a constant (Eqs.(24) and (28)) and using Eq. (45) we have

$$\sigma(z) = \frac{E(z)}{\int_{-h/2}^{h/2} E(z)dz} P_x \tag{47}$$

Making use of the PWED model, the denominator on the RHS can further be determined as

$$\int_{-h/2}^{h/2} E(z)dz = \sum_{i=1}^{L}\int_{h_{i-1}}^{h_i} E_i(z)dz \approx \sum_{i=1}^{L}\int_{h_{i-1}}^{h_i} a_{Ei}(b_{Ei})^z dz = \sum_{i=1}^{L}\frac{a_{Ei}}{Inb_{Ei}}\left((b_{Ei})^{h_i} - (b_{Ei})^{h_{i-1}}\right) \tag{48a}$$

and

$$\sigma_{ip}(z) = \frac{a_{Ei}(b_{Ei})^z}{\sum\limits_{i=1}^{L}\frac{a_{Ei}}{Inb_{Ei}}\left((b_{Ei})^{h_i}-(b_{Ei})^{h_{i-1}}\right)}P_x \quad , \tag{48b}$$

i=1, …, L.

(2) Purely elastic solution of the stress distribution$\sigma_\theta$caused by $\Delta\bar{\theta}$.

When $\Delta\bar{\theta}$ is applied individually, assuming the plate is free in z-direction, one can obtain

$$\int_A \sigma_x dA = 0. \tag{49}$$

Keeping in mind that

$$\varepsilon(z) = \varepsilon_0, \tag{50}$$

substituting Eqs. (50) and (45) into Eq. (49) yields

$$\varepsilon(z) = \varepsilon_0 = (1+\nu)\frac{\int_{-h/2}^{h/2}\alpha(z)E(z)\Delta\theta(z)dz}{\int_{-h/2}^{h/2}E(z)dz} \tag{51}$$

Combining Eq. (51) with Eq. (45), the thermal stress field can be determined as

$$\sigma(z,\Delta\bar{\theta}) = \sigma_x|_{P_x=0} = \frac{E(z)}{1-\nu}\left[\frac{\int_{-h/2}^{h/2}\alpha(z)E(z)\Delta\theta(z)dz}{\int_{-h/2}^{h/2}E(z)dz} - \alpha(z)\Delta\theta(z)\right] \tag{52a}$$

Making use of the PWED model, the distribution of the thermal stress can be obtained as

$$\sigma_{i\theta}(z,\Delta\bar{\theta}) = \frac{E_i(z)}{1-\nu}\left[\frac{\sum\limits_{i=1}^{L}\int_{h_{i-1}}^{h_i}\alpha_i(z)E_i(z)\Delta\theta_i(z)dz}{\sum\limits_{i=1}^{L}\int_{h_{i-1}}^{h_i}E_i(z)dz} - \alpha_i(z)\Delta\theta_i(z)\right], \tag{52b}$$

i=1, ..., L.

Substituting Eq.(20a), Eq.(22a) and Eq.43(a) into Eq.(52b), one can obtain

$$\sigma_{i\theta}(z,\Delta\bar{\theta}) = \Delta\bar{\theta} f_i(z), \tag{53a}$$

i=0, 1, ..., L.

Where

$$f_i(z) = \frac{a_{Ei} b_{Ei}^z}{1-\nu}\left[\frac{\sum_{i=1}^{L}\int_{h_{i-1}}^{h_i} a_{\alpha i}a_{Ei}\left(b_{\alpha i}b_{Ei}\right)^z\left(a_{\theta i}+b_{\theta i}\bar{b_{\lambda i}^{z}}\right)dz}{\sum_{i=1}^{L}\int_{h_{i-1}}^{h_i} a_{Ei}b_{Ei}^z dz} - a_{\alpha i}b_{\alpha i}^z\left(a_{\theta i}+b_{\theta i}\bar{b_{\lambda i}^{z}}\right)\right] \tag{53b}$$

Comparing with Eq.(49), one can obtain $\sum_{i=1}^{L}\int_{h_{i-1}}^{h_i} f_i(z)\,dz = 0$. And the denominator on the right hand side of Eq. (53b) can be expressed as

$$\begin{aligned}&\sum_{i=1}^{L}\int_{h_{i-1}}^{h_i} a_{\alpha i}a_{Ei}\left[a_{\theta i}\left(b_{Ei}b_{\alpha i}\right)^z + b_{\theta i}\left(\frac{b_{Ei}b_{\alpha i}}{b_{\lambda i}}\right)^z\right]dz \Big/ \sum_{i=1}^{L}\int_{h_{i-1}}^{h_i} E_i(z)\,dz \\ &= \frac{\sum_{i=1}^{L}\left\{\frac{a_{\alpha i}a_{Ei}a_{\theta i}}{In\left(b_{Ei}b_{\alpha i}\right)}\left[\left(b_{Ei}b_{\alpha i}\right)^{h_i}-\left(b_{Ei}b_{\alpha i}\right)^{h_{i-1}}\right]+\frac{a_{\alpha i}a_{Ei}b_{\theta i}}{In\left(b_{Ei}b_{\alpha i}\right)-In\left(b_{\lambda i}\right)}\left[\left(\frac{b_{Ei}b_{\alpha i}}{b_{\lambda i}}\right)^{h_i}-\left(\frac{b_{Ei}b_{\alpha i}}{b_{\lambda i}}\right)^{h_{i-1}}\right]\right\}}{\sum_{i=1}^{L}\frac{a_{Ei}}{Inb_{Ei}}\left(b_{Ei}^{h_i}-b_{Ei}^{h_{i-1}}\right)}\end{aligned} \tag{53c}$$

3.6 Static shakedown of Bree plate

The shakedown analysis of the Bree plate includes the determination of the boundary of initial yield, the boundary between the areas of shakedown and incremental collapse, and the boundary between the areas of shakedown and reversed plasticity.

The plate will have two parts, in one part there will be $f_i(z) \le 0$, then in the other part there will be $f_i(z) \ge 0$. From the temperature distribution which has been given by Fig. 1 and constant mechanical load condition, one can obtain the expressions of shakedown boundaries of the plate.

(1) Initial yield

Namely, no plastic deformation takes place provided

$$\sigma_{iP}(z) + \sigma_{i\theta}(z,\Delta\bar{\theta}) \le \sigma_{iy}^0(z) \text{ for } f_i(z) \ge 0,\ i = 0,1,\ldots,L. \tag{54a}$$

$$\sigma_{iP}(z) + \sigma_{i\theta}(z,\Delta\bar{\theta}) \ge -\sigma_{iy}^0(z) \text{ and } \sigma_{iP}(z) \le \sigma_{iy}^0(z) \quad \text{for } f_i(z) \ge 0,\ i = 0,1,\ldots,L. \tag{54b}$$

(2) Static shakedown boundaries

Suppose there are a time-independent residual stress fields $\bar{\rho}_{ix}(z)$ and a time-independent field $k^*(1 \le k^* \le d)$ in the plate, with the same as initial yield analysis, the plate may shakedown if the following condition is satisfied in one temperature change cycle

$$\begin{aligned} &\sigma_{iP}(z) + \sigma_{i\theta}(z, \Delta\tilde{\theta}) + \bar{\rho}_{ix}(z) \le \sigma_{iy}(z) \\ &\sigma_{iP}(z) + \bar{\rho}_{ix}(z) \ge -\sigma_{iy}(z) \end{aligned} \quad \text{for } f_i(z) \ge 0,\ i = 0, 1, \ldots, L. \tag{55a}$$

$$\begin{aligned} &\sigma_{iP}(z) + \sigma_{i\theta}(z, \Delta\tilde{\theta}) + \bar{\rho}_{ix}(z) \ge -\sigma_{iy}(z) \\ &\sigma_{iP}(z) + \bar{\rho}_{ix}(z) \le \sigma_{iy}(z) \end{aligned} \quad \text{for } f_i(z) \le 0,\ i = 0, 1, \ldots, L, \tag{55b}$$

where $\sigma_{iy}(z) = k^* \sigma_{iy}^0(z)$.

The shakedown boundaries of the plate include two parts: the boundary between the area of shakedown and that of incremental collapse, and the boundary between the area of shakedown and that of reversed plasticity.

(a) Shakedown boundary corresponding to reversed plasticity

It can be obtained from Ineq. (55) that

$$\sigma_{i\theta}(z, \Delta\bar{\theta}) \le 2\sigma_{iy}(z), \quad f_i(z) \ge 0,\ i = 0, 1, \ldots, L. \tag{56a}$$

$$\sigma_{i\theta}(z, \Delta\bar{\theta}) \ge -2\sigma_{iy}(z), \quad f_i(z) \le 0,\ i = 0, 1, \ldots, L. \tag{56b}$$

The equality of both sides of any one of Ineq. (56) at any point in the cross section implies the equality of both sides of Ineqs. $(55a)_1$ and $(55a)_2$, or the equality of Ineqs. $(55b)_1$ and $(55b)_2$, indicating that reversed plasticity occurs to this point in the cross section.

(b) Shakedown boundary corresponding to incremental collapse

Making use of the given time-independent residual stress field $\bar{\rho}_{ix}(z)$ and noticing that $\Delta\tilde{\theta} = \Delta\bar{\theta}$ as $n\Delta t \le t \le (n{+}0.5)\Delta t$, Ineq. (55) can be rewritten in this duration as

$$\sigma_{iP}(z) + \sigma_{i\theta}\left(z, \Delta\bar{\theta}\right) + \bar{\rho}_{ix}(z) = \sigma_{iy}(z) \text{ for } f_i(z) \ge 0,\ i = 0, 1, \ldots, L, \tag{57a}$$

$$\sigma_{iP}(z) + \sigma_{i\theta}(z, \Delta\bar{\theta}) + \bar{\rho}_{ix}(z) \le -\sigma_{iy}(z) \text{ for } f_i(z) \ge 0,\ i = 0, 1, \ldots, L, \tag{57b}$$

while since $\Delta\tilde{\theta} = 0$ as $(n{+}0.5)\Delta t \le t \le (n{+}1)\Delta t$, In eq. (55) should be reduced in this duration to

$$\sigma_{iP}(z) + \bar{\rho}_{ix}(z) \ge -\sigma_{iy}(z) \text{ for } f_i(z) \ge 0,\ i = 0, 1, \ldots, L. \tag{57c}$$

$$\sigma_{iP}(z) + \bar{\rho}_{ix}(z) = \sigma_{iy}(z) \text{ for } f_i(z) \le 0,\ i = 0, 1, \ldots, L. \tag{57d}$$

In eqs. (57) indicates that at each point in the region where $f_i(z) \geq 0$ of the cross section, the stress $\sigma_+ = \sigma_{iP}(z) + \sigma_{i\theta}(z, \Delta\bar{\theta}) + \bar{\rho}_{ix}(z)$ reaches $\sigma_{iy}(z)$; while at each point in the region where $f_i(z) \leq 0$ of the cross section, the stress $\sigma_- = \sigma_{iP}(z) + \bar{\rho}_{ix}(z)$ reaches $\sigma_{iy}(z)$. That is, in $n\Delta t \leq t \leq$ (n+0.5)Δt, σ_+ at a part of the Bree plate reaches $\sigma_y(z)$, and in (n+0.5)$\Delta t \leq t \leq$ (n+1)Δt, σ_- at the other part of the Bree plate reaches $\sigma_y(z)$. The two parts of the cross section may flow forward alternatively.

3.7 Kinematic shakedown analysis of Bree plate

Given a kinematically permissible strain increment$\Delta\bar{\varepsilon}$we obtain the following relationships from Eq. (14)

$$J_{Pi}(z) = \sigma_{iP}(z)\Delta\varepsilon, \quad \beta_P^- = 0, \quad \beta_P^+ = 1, \quad i = 0, 1, \ldots, L. \tag{58a}$$

$$J_{\theta i}(z) = \sigma_{i\theta}\left(z, \Delta\bar{\theta}\right)\Delta\varepsilon \quad \beta_\theta^- = 0, \quad \beta_\theta^+ = 1, \quad i = 0, 1, \ldots, L. \tag{58b}$$

Keeping in mind $P_x \geq 0$ and Eq.(48b), namely $\sigma_{iP}(z) \geq 0$, so that $\alpha_P = \beta_P^+ = 1$. Because $\sigma_{i\theta}\left(z, \Delta\bar{\theta}\right) \leq 0$ at $f_i(z) \leq 0$ and $\sigma_{i\theta}\left(z, \Delta\bar{\theta}\right) \geq 0$ at $f_i(z) \geq 0$, so we define

$$g_i(z) = \begin{cases} f_i(z), & f_i(z) \geq 0, \\ 0, & f_i(z) \leq 0, \end{cases} \quad i = 0, 1, \ldots, L. \tag{59}$$

Substituting Eqs.(48b), (53a) and (59) into Eq.(14), one can obtain

$$k^* \sum_{i=1}^{L} \int_{h_{i-1}}^{h_i} \sigma_{yi}^0(z)dz \geq \sum_{i=1}^{L} \int_{h_{i-1}}^{h_i} \sigma_{iP}(z)dz + \Delta\bar{\theta} \sum_{i=1}^{L} \int_{h_{i-1}}^{h_i} g_i(z)dz \tag{60}$$

where

$$\sum_{i=1}^{L} \int_{h_{i-1}}^{h_i} \sigma_{iy}^0(z)dz \approx \sum_{i=1}^{L} \int_{h_{i-1}}^{h_i} a_{yi} b_{yi}^z dz = \sum_{i=1}^{L} \frac{a_{yi}}{Inb_{yi}} \left(b_{yi}^{h_i} - b_{yi}^{h_{i-1}}\right) \tag{61}$$

$$\sum_{i=1}^{L} \int_{h_{i-1}}^{h_i} \sigma_{ip}(z)dz = \sum_{i=1}^{L} \int_{h_{i-1}}^{h_i} \frac{E_i(z)}{\sum_{j=1}^{L} \int_{h_{j-1}}^{h_j} E_j(z)dz} P_x dz = P_x \tag{62}$$

And we evaluate $\sum_{i=1}^{L} \int_{h_{i-1}}^{h_i} g_i(z)dz$ numerically. So Eq.(60) can be given as

$$k^* \sum_{i=1}^{L} \frac{a_{yi}}{Inb_{yi}} \left(b_{yi}^{h_i} - b_{yi}^{h_{i-1}}\right) \geq P_x + \Delta\bar{\theta} \sum_{i=1}^{L} \int_{h_{i-1}}^{h_i} g_i(z)dz \tag{63}$$

Then given $\Delta\bar{\theta}$, the corresponding P_x can easily be derived from Eqs. (63).

4 Application to shakedown analysis of FGP

4.1 Effective properties of the FGP

The FG plate is assumed to be made of functionally graded Al/SiC composite, containing elastoplastic aluminum matrix reinforced with linearly elastic SiC particles. The thermal and mechanical properties of each constituent [Shen (1998)] are listed in Table 1. For the given yield and ultimate strengths of the aluminum, i.e., σ_y and σ_u, d=2.32 can be determined for the matrix material.

Table 1: Material constants of constituents.

Constituent	E (GPa)	ν	α ($10^{-6}\mathrm{K}^{-1}$)	σ_y (MPa)	σ_u (MPa)	λ (W/K.m)
Al(matrix)	69	0.33	23.1	34	79	237
SiC(inclusion)	450	0.17	4.7	—	—	368

We assumed the thickness of the plate h=60mm, it is separated into L=20 segments with identical increment, so h_0=-h/2, h_1=-h/2+h/20, ..., h_i=-h/2+ih/20,..., h_{20}=h/2. The particle volume fraction,$\xi(z)$, is assumed to be distributed linearly as

$$\xi(z) = \frac{3}{10}\left(\frac{1}{2}+\frac{z}{h}\right). \tag{64}$$

The effective thermal and mechanical properties of the FG plate are calculated respectively with Eqs. (27), (29), (35) and (36) and shown in Fig. 4. It can be seen that the piecewise exponential distribution model can satisfactorily describe the distribution of the material properties.

4.2 Static and kinematic shakedown analysis

Although, in principle, the lower bound of the shakedown loads of a structure can be determined by simply assuming a residual stress field, in order to illustrate the importance of an appropriate shakedown analysis of FG structures, more accurate shakedown boundary is to be achieved by considering in details the effect of the nonlinearity and the heterogeneity of the involved material properties on the shakedown of the FG structure.

The boundary of elasticity is determined with Ineqs. (54) and shown in Fig. 5 with the lines marked with (E-S). It can be seen that, different from that of the conventional Bree plate [Bree (1967)], the boundary consists of three segments, determined by Ineqs. (54a), (54b)$_1$ and (54b)$_2$, respectively. In segment AB, the capability for the plate to carry P_x is enhanced with the increase of temperature

change $\Delta\bar{\theta}$. In segment BC,P_x increases with the decrease of $\Delta\bar{\theta}$. In order to illustrate these phenomena, the distributions of σ_P,σ_θ,$\sigma=\sigma_P+\sigma_\theta$ and σ_y^0 at Point A at the loading state, B, and C (Fig. 5) are plotted in Figs. 6(a) and (b), respectively, where the zone bounded by "*" denotes the elastic zone. At Point A, P_x=0 and $\sigma=\sigma_\theta$ reaches $-\sigma_y^0$at $z=-h/2$. With the increase of P_x, σ_P increases so that σ_θ at $z=-h/2$ should decrease due to the yield condition $\sigma=\sigma_P+\sigma_\theta=-\sigma_y^0$, indicating the increase of $\Delta\bar{\theta}$. This trend will be kept until Point B (Ineq. $(57b)_1$). At the same time, the increase of either P_x or $\Delta\bar{\theta}$ will increase the stress $\sigma=\sigma_P+\sigma_\theta$ at z=$h/2$, this tendency continues until $\sigma=\sigma_P+\sigma_\theta=\sigma_y^0$ is satisfied at z=$h/2$, corresponding to the critical point B in Fig. 5 with the stress distributions shown in Fig. 6(b). After Point B the plate will no longer be elastic with the further increase of $\Delta\bar{\theta}$. If both P_x and $\Delta\bar{\theta}$ change by segment BC in Fig. 5 (Ineq. (54a)), the material at z=h/2 will keep yielding while the material at z=-h/2 turns to elastic, and this process continues up to Point C (Fig. 5).

First, let $\sigma_+=\sigma_P+\bar{\rho}_x+\sigma_\theta$ and $\sigma_-=\sigma_P+\bar{\rho}_x$ which will be given in the following figures. In the following analysis, $k^*=d$ is chosen and $\sigma_y=d\cdot\sigma_y^0$.

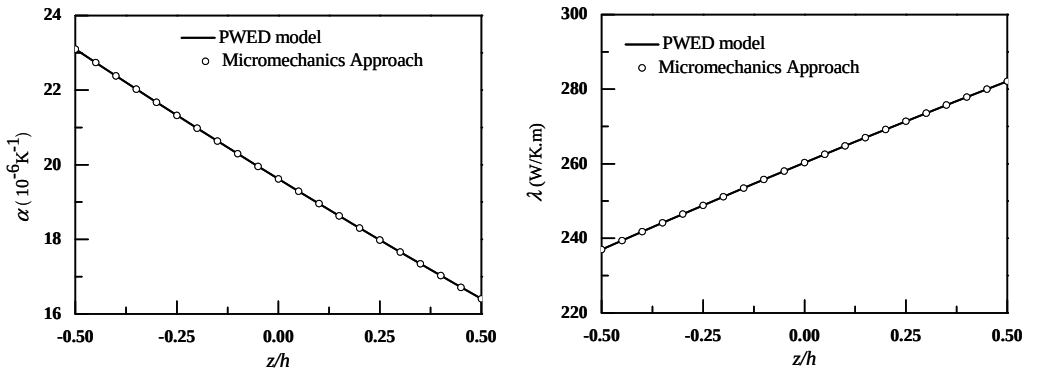

(c) CTE (d) Thermal Conductivity

Figure 4: Mechanical and thermal properties of Al/Sic FG plate

The boundary between the area of shakedown and that of reversed plasticity is given in Fig. 5 with the curve marked with (S-RP) determined by Ineqs. (56a) and (56b). The distributions of the residual stress $\bar{\rho}_x$, the stress σ_P, σ_θ, σ_+ and σ_- at Point E in Fig. 5 are shown in Fig. 7(b), where the boundary marked with "*" denotes the elastic zone, within which the accumulation of plastic deformation is limited, but plastic deformation may take place if either σ_+ and σ_- reaches the boundary. Making use of the residual stress field shown in Fig. 7(a), in the duration

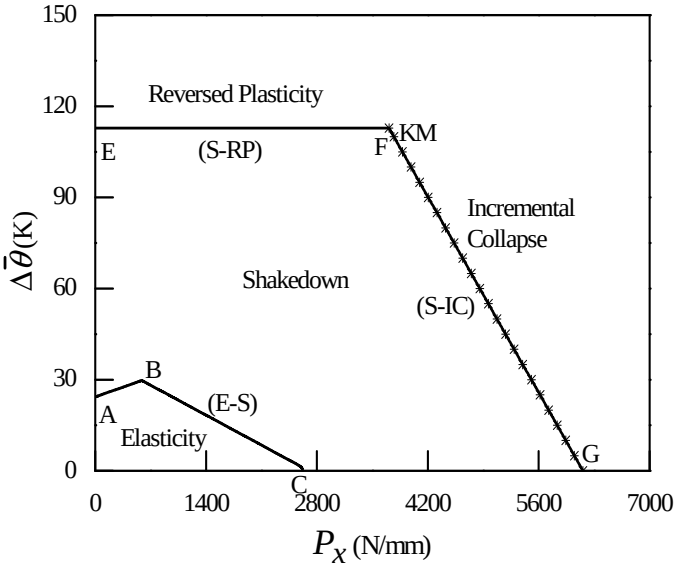

Figure 5: Shakedown area of the FG Bree plate

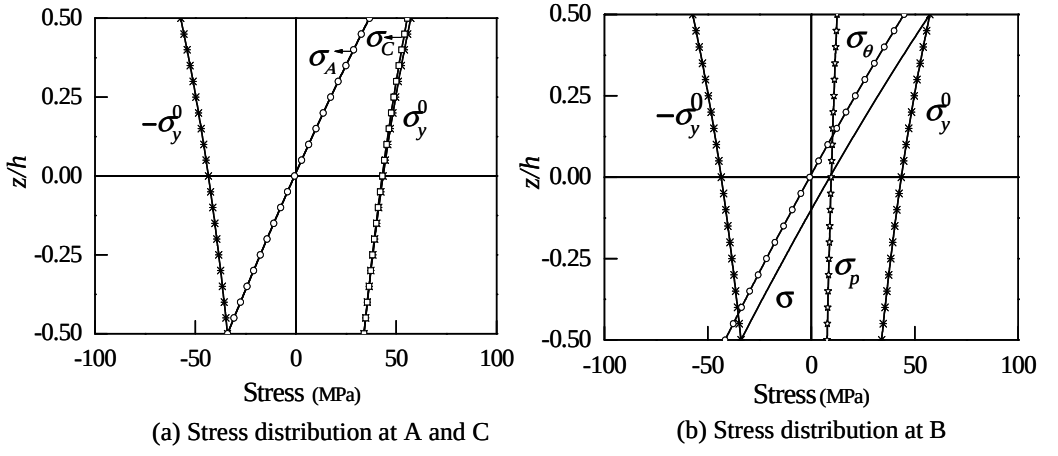

(a) Stress distribution at A and C

(b) Stress distribution at B

Figure 6: Stress distributions at points A, B, and C (Fig. 5)

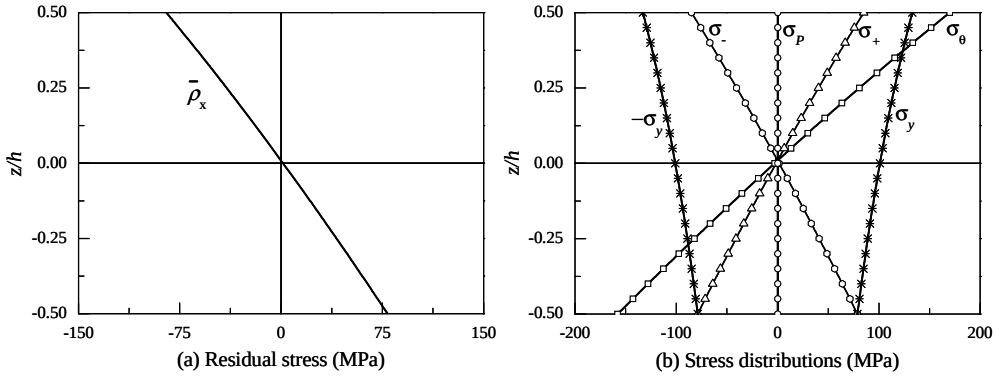

Figure 7: Stress distributions at points E

$n\Delta t \leq t \leq (n+0.5)\Delta t$ as $\Delta\bar{\theta}$ is applied, the obtained σ_+ reaches $-\sigma_y$ at z=-h/2 ; and in the duration $(n+0.5)\Delta t \leq t \leq (n+1)\Delta t$ as $\Delta\bar{\theta}$ is removed, the obtained σ_- reaches σ_y at z=-h/2, indicating that reversed plastic deformation may take place at this location. It should be noted that, similar situation also will occur at Point F (Fig. 5), the intersection point of line (S-IC) and line (S-RP), corresponds to the thermal-mechanical loads resulting in overall incremental collapse and local reversed plasticity.

The boundary between shakedown and incremental collapse regions can be determined with Ineq. (57) by the following steps: (1) Given a set of $\Delta\bar{\theta}$ and P_x, the residual stress field$\bar{\rho}_x$can be estimated with Eqs.(57a) and (57d); (2) Check if the obtained $\bar{\rho}_x$ satisfies the Ineqs.(57b) and (57c); (3) Check if the residual stress field $\bar{\rho}_x$ satisfies the self-equilibrium condition; (4) If the step (2) or (3) is not satisfied, adjust P_x and then return to step (1).

The determined boundary between shakedown and incremental collapse regions is shown in Fig. 5 with the line marked with (S-IC). The distributions of the residual stress $\bar{\rho}_x$, the stress σ_P, σ_θ and σ_+ at Point F in Fig. 5 are shown in Fig. 8. Using of the residual stress field shown in Fig.8 (a), the stress σ_+ will reach σ_y in the region $f_i(z) \geq 0$ as $\Delta\bar{\theta}$ is applied during $n\Delta t \leq t \leq (n+0.5)\Delta t$, But in the opposite direction, σ_+ does not reach the yield criterion except at z=-h/2, implying that no overall plastic deformation takes place in the direction of σ_+. And in (n+0.5)$\Delta t \leq t \leq$(n+1)$\Delta t\sigma_-$ reaches σ_y in the other region. Therefore, plastic flow takes place in the direction of σ_+ in the region $f_i(z) \geq 0$ during $n\Delta t \leq t \leq$(n+0.5)Δt, i.e., plastic deformation develops in each cycle of$\Delta\bar{\theta}$ and increases monotonically with the increase of n. It should be noted that in the opposite direction, σ_+ also reaches $-\sigma_y$

at z=-h/2, indicating that reversed plastic deformation may occur at z=-h/2. It can also be seen in Fig. 5, where Point F is found to be the intersection of the boundary between shakedown and incremental collapse and that between shakedown and reversed plasticity.

Different from the results shown in Fig. 8, the distributions of stress at Point G (Fig. 5) are shown in Fig. 9, corresponding to $\Delta\bar{\theta} = 0$. Making use of the residual stress $\bar{\rho}_x$ shown in Fig. 9(a), one can obtain the stress distributions of the plate shown in Fig. 9(b). It can be seen that in the whole duration of $n\Delta t \leq t \leq (n+1)\Delta t$, $\sigma = \sigma_P(z) + \bar{\rho}_x(z)\,\theta$ reaches $\sigma_y(z)$, namely in the plate the stress totally reaches the utmost stress.

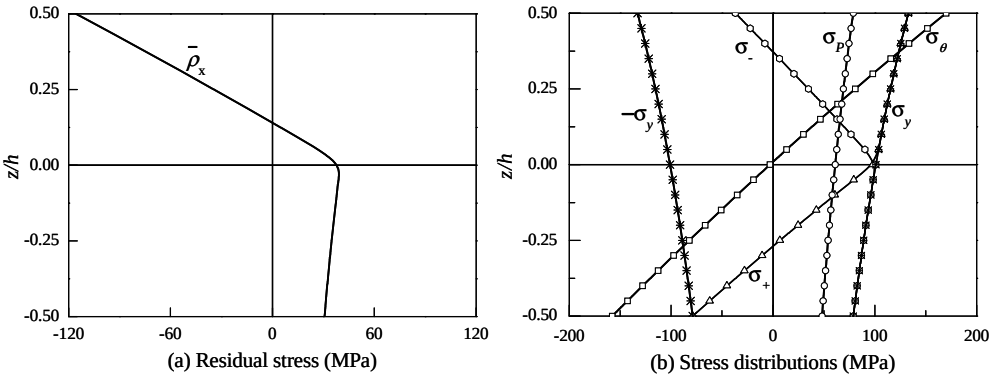

Figure 8: Stress distributions at Point F

The kinematic shakedown boundary determined with Ineq. (63) is also given in Fig. 5 with the line marked with KM. It coincides well with the boundary marked with (S-IC) determined by the static shakedown theorem, indicating that the boundary S-IC should be the realistic shakedown boundary of this plate.

5 Conclusions and discussion

The static and kinematic shakedown of an FG Bree plate is analyzed. The material is assumed linearly elastic and non-linear isotropic hardening. The plate is subjected to coupled constant mechanical load and cyclically varying temperature. In order to make the analysis more accurate, the pair-wise interaction micromechanical approximation is used for the evaluation of the effective properties of composite materials, and the piece-wise exponential distribution model is used to simulate their distribution in an FG plate. The shakedown area in the load domain is

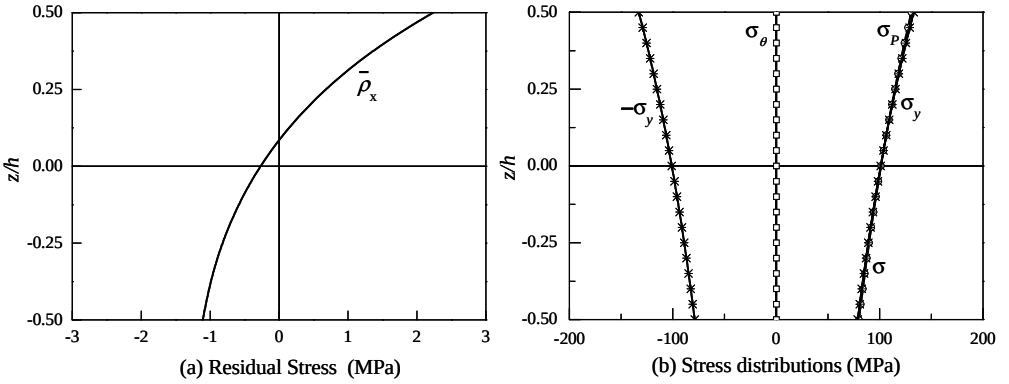

Figure 9: Stress distributions at points G

determined and the stress distributions under some typical loading conditions are analyzed. The following conclusions are drawn from the analysis:

(1) The effective mechanical properties of the FG plate are determined with the micromechanics-based model which takes into account direct pair-wise particles interactions, which can be computed and implemented conveniently with Eqs. (25)-(29). In FGMs, the volume fraction of particles may be very large, indicating the significance of the interaction between particles. In this article, the interaction between particles was introduced directly with a pair-wise interaction model for evaluating the mechanical properties of FG plate, which, together with the piecewise-exponential distribution model, may yield more realistic replication of the thermal-mechanical properties of materials and their distributions.

(2) The piecewise exponential distribution model adopted can replicate the distribution of the actual properties of the FG plate with sufficient accuracy. And on the other hand, it can easily be applied because it also coincides with the discrete approach used in the numerical analysis. Since the actual material properties in FG structures may be complicated and difficult to be represented with a conventional predefined simple function, the piecewise distribution model is of special advantages.

(3) The thermal-mechanical property of an FG structure is closely related to the distributions of material properties, which implies the possibility to enhance its load-bearing capability by optimizing the properties of the attendant constituents as well as the distributions of overall material properties.

(4) FGMs are usually used in the structures subjected to severe coupled thermal and

mechanical loading and shakedown is an essential problem for such application. The approach developed and the results obtained can, therefore, provide available information for the analysis and design of such kind of structures.

Acknowledgement: The authors gratefully acknowledge the financial support to this work from NSFC under Grant Numbers 11272364.

References

Aboudi, J.; Pindera, M.J.; Arnold, S.M. (1999): Higher-order theory for functionally graded materials. *Composites: B*, 30: 777-832.

Aghababaei, R.; Reddy, J.N. (2009): Nonlocal third-order shear deformation plate theory with application to bending and vibration of plates. *Journal of Sound and Vibration*, 326: 277–289.

Altenbach, H.; Eremeyev, V.A. (2009): Eigen-vibrations of plates made of functionally graded material. *CMC: Computers, Materials, & Continua*, 9: 153-178.

Andrew, J.G.; Senthil, S.V. (2010): Transient multiscale thermoelastic analysis of functionally graded materials. *Composite Structures*, 92: 1372-1390

Bree, J. (1967): Elastic plastic behavior of thin tubes subjected to internal pressure and intermittent high heat fluxes with application to fast nuclear reactor fuel elements. *Journal of Strain Analysis*, 2: 226-238.

Budiansky, B. (1965): On the elastic moduli of some heterogeneous materials. *Journal of the Mechanics and Physics of Solids*, 13: 223-227.

Cheng, Z.Q.; Batra, R.C. (2000): Three-dimensional thermoelastic deformations of a functionally graded elliptic plate. *Composites: Part B*, 31: 97-106.

Cho, J.R.; Oden, J.T. (2000): Functionally graded material: a parametric study on thermal-stress characteristics using the Crank-Nicolson-Galerkin scheme. *Computer Methods in Applied Mechanics and Engineering*, 188: 17-38.

Elishakoff, I.; Gentilini, C. (2005): Three-dimensional flexure of rectangular plates made of functionally graded materials. *Journal of Applied Mechanics*, 72: 788-791.

Feldoman, E.; Aboudi, J. (1997): Buckling analysis of functionally graded plates subjected to uniaxial loading. *Composite Structures*, 38: 29-36.

Gasik, M.M. (1998): Micromechanical modeling of functionally graded materials. *Computational Materials Science*, 13: 42-55.

Gilhooley, D.F.; Batra, R.C.; Xiao, J.R.; Mccarthy, M.A.; Gillespie, J.W. (2007): Analysis of thick functionally graded plates by using higher-order shear and normal deformable plate theory and MLPG method with radial basis functions. *Composite*

Structures, 80: 539-552.

Guo, L.C.; Noda, N. (2007): Modeling method for a crack problem of functionally graded materials with arbitrary properties piecewise exponential model. *International Journal of Solids and Structures*, 44: 6768-6790.

Guo, L.C.; Noda, N. (2008a): Fracture mechanics analysis of functionally graded layered structures with a crack crossing the interface. *Mechanics of Materials*, 40: 81-99.

Guo, L.C.; Noda, N.; Wu, L. (2008b): Thermal fracture model for a functionally graded plate with a crack normal to the surfaces and arbitrary thermomechanical properties. *Composites Science and Technology*, 68: 1034-1041.

Guo, L.; Wu, L.; Sun, Y.; Ma, L. (2005): The transient fracture behavior for a functionally graded layered structure subjected to an in-plane impact load. *Acta Mechanica Sinica*, 21: 257-266.

Hasselman, D.P.H.; Youngblood, G.E. (1978): Enhanced thermal stress resistance of structural ceramics with thermal conductivity gradient. *Journal of the American Ceramic Society*, 61: 49-53.

Hill, R. (1965): A self-consistent mechanics of composite materials. *Journal of the Mechanics and Physics of Solids*, 13: 213-222.

Hosseini, S.M.; Shahabian, M.; Sladek, J.; Sladek, V. (2011): Stochastic Meshless Local Petrov-Galerkin (MLPG) method for thermo-elastic wave propagation analysis in functionally graded thick hollow cylinders. *CMES: Computer Modeling in Engineering & Sciences*, 71(1): 39-66.

Ju, J.W.; Chen, T.M. (1994a): Micromechanics and effective elastoplastic behavior of two-phase metal matrix composites. *Journal of Engineering Materials and Technology*, 116: 310-318.

Ju, J.W.; Chen, T.M. (1994b): Micromechanics and effective moduli of elastic composites containing randomly dispersed ellipsoidal inhomogeneities. *Acta Mechanica*, 103: 103-121.

Ju, J.W.; Chen, T.M. (1994c): Effective elastic moduli of two-phase composites containing randomly dispersed spherical inhomogeneities. *Acta Mechanica*, 103: 123-144.

Kim, J.H.; Paulino, G.H. (2003): An accurate scheme for mixed-mode fracture analysis of functionally graded materials using the interaction integral and micromechanics models. *International Journal for Numerical Methods in Engineering*, 58: 1457-1497.

König, J.A. (1987): Shakedown of elastic-plastic Structures. *PWN-Polish Scientific Publichers*.

Koizumi, M. (1993): The concept of FGM. Ceramic transactions. *Functionally Gradient Material*, 34: 3-10.

Miyamoto, Y.; Kaysser, W.A.; Rabin, B.H.; Kawasaki, A.; Ford, R.G. (1999): Functionally graded materials: design, processing and applications. *Kluwer Academic Publishers, Dordrecht*.

Mori, T.; Tanaka, K. (1973): Average stress in matrix and average elastic energy of materials with misfitting inclusions. *Acta Metallurgica*, 21: 571-574.

Na, K.S.; Kim, J.H. (2006): Three-dimensional thermomechanical buckling analysis for functionally graded composite plates. *Composite Structures*, 73: 413-422.

Peng, X.; Fan, J.; Zeng, X. (1996): Analysis for plastic buckling of thin-walled cylinders via non-classical constitutive theory of plasticity. *International Journal of Solids and Structures*, 33: 4495-4509.

Peng, X.; Ponter, A.R.S. (1993): Extremal properties of Endochronic plasticity, Part II: Extremal path of the Endochronic constitutive equation with a yield surface and application. *International Journal of Plasticity*, 9: 567-581.

Peng, X.; Hu N.; Zheng, H.; Fang, C. (2009a): Analysis of shakedown of FG Bree plate subjected to coupled thermal-mechanical loadings. *Acta Mechanica Solida Sinica*, 22: 95-108.

Peng, X.; Zheng, H.; Hu, N.; Fang, C. (2009b): Static and kinematic shakedown analysis of FG plate subjected to constant mechanical load and cyclically varying temperature change. *Composite Structures*, 91: 212-221.

Reddy, J.N. (2004): Mechanics of Laminated Composite Plates and Shells: Theory and Analysis. *Second Edition. CRC Press, Boca Raton, FL.*

Reddy, J.N. (2011): Microstructure-dependent couple stress theories of functionally graded beams. *Journal of the Mechanics and Physics of Solids*, 59: 2382-2399.

Reiter, T.; Dvorak, G..J. (1998): Micromechanical models for graded composite materials: II. Thermomechanical loading. *Journal of the Mechanics and Physics of Solids*, 46: 1655-1673.

Reiter, T.; Dvorak, G.J.; Tvergaard, V. (1997): Micromechanical models for graded composite materials. *Journal of the Mechanics and Physics of Solids*, 45: 1281-1302.

Shen, Y.L. (1998): Thermal expansion of metal-ceramic composites: a three-dimensional analysis. *Materials Science & Engineering A*, 252: 269-275

Suresh, S.; Mortensen, A. (1998): Fundamentals of functionally graded materials. *IOM Communications Ltd, London.*

Suresh, S.; Mortensen, A. (1998): Fundamentals of functionally graded materials.

London, UK: Institute of Materials.

Tian, J.H.; Han, X.; Long, S.Y.; Xie, G.Q. (2009): An analysis of the heat conduction problem for plates with the functionally graded material using the hybrid numerical method. *CMC: Computers, Materials, & Continua*, 10: 229-242.

Tian, J.H.; Han, X.; Long, S.Y.; Sun, G.Y.; Cao Y.; Xie, G.Q. (2010): An analysis of the transient heat conduction for plates with the functionally graded material using the hybrid numerical method. *CMES: Computer Modeling in Engineering & Sciences*, 63(2): 101-116.

Vel, S.S.; Batra, R.C. (2002): Exact solution for thermoelastic deformations of functionally graded thick rectangular plates. *AIAA Journa*l, 40: 1421-1433.

Vel, S.S.; Batra, R.C. (2003): Three-dimensional analysis of transient thermal stresses in functionally graded plates. *International Journal of Solids and Structures*, 40: 7181-7196.

Wang, B.L.; Han, J.C.; Du, S.Y. (2000): Crack problems for functionally graded materials under transient thermal loading. *Journal of Thermal Stresses*, 23: 143-168.

Watari, F.; Yokoyama, A.; Omori, M.; et al. (2004): Biocompatibility of materials and development to functionally graded implant for biomedical application. *Composites Science and Technology*, 64: 893-908.

Wu, C.P.; Huang, S.E. (2009): Three-dimensional solutions of functionally graded piezo-thermo- elastic shells and plates using a modified Pagano method. *CMC: Computers, Materials, & Continua*, 12: 251-282.

Yamanouchi, M.; Koizumi, M.; Hirai, T.; Shiota, I. (Eds.). (1990): Proceedings of the First International Symposium on Functionally Gradient Materials. Japan.

Yin, H.M.; Paulino, G.H.; Buttlar, W.G.; Sun, L.Z. (2005): Effective thermal conductivity of functionally graded particulate composites. *Journal of Applied Physics*, 98: 063704.

Yin, H.M.; Paulinoa, G.H.; Buttlara, W.G.; Sun, L.Z. (2007): Micromechanics-based thermoelastic model for functionally graded particulate materials with particle interactions. *Journal of the Mechanics and Physics of Solids*, 55: 132-160

Yin, H.M.; Sun, L.Z.; Paulino, G.H. (2004): Micromechanics-based elastic modeling for functionally graded materials with particle interactions. *Acta Materialia*, 52: 3535–3543.

Zhong, Z.; Shang, E.T. (2003): Three-dimensional exact analysis of simply supported functionally gradient piezoelectric plates. *International Journal of Solids and Structures*, 40: 5335-5352.

Zuiker, J.R. (1995): Functionally graded materials: choice of micromechanics

model and limitations in property variation. *Composites Engineering*, 5: 807-819.

Zuiker, J.R.; Dvorak, G.J. (1994): The effective properties of functionally graded composites—I. Extension of the Mori–Tanaka method to linearly varying fields. *Composites Engineering*, 4: 19-35.